



# Low-temperature conducting performance of transparent indium tin oxide/antimony tin oxide electrodes



Bon-Ryul Koo<sup>a</sup>, Ju-Won Bae<sup>b</sup>, Hyo-Jin Ahn<sup>a,b,\*</sup>

<sup>a</sup> Program of Materials Science & Engineering, Convergence Institute of Biomedical Engineering and Biomaterials, Seoul National University of Science and Technology, Seoul 139-743, Republic of Korea

<sup>b</sup> Department of Materials Science and Engineering, Seoul National University of Science and Technology, Seoul 139-743, Republic of Korea

## ARTICLE INFO

### Keywords:

Transparent conducting oxides  
Surface  
Electrical properties  
Optical properties  
Electrodes

## ABSTRACT

We fabricated transparent indium tin oxide (ITO)/antimony tin oxide (ATO) electrodes using a combined process of spin-coating of hybrid ITO nanoinks, electrospinning of ATO, and hydrogen (H<sub>2</sub>) activation carried out at a low annealing temperature of 200 °C. The produced ITO electrode exhibited an enhanced surface densification and phase conversion of In(OH)<sub>3</sub> to ITO. As a result, the H<sub>2</sub>-activated ITO/ATO electrodes exhibited excellent transparent conducting performances with a superior sheet resistance of ~47.5 Ω/□ and a good transmittance of ~85.3% as compared to the ITO and ITO/ATO electrodes. Despite the use of the low annealing temperature, the achieved improvement in the conducting performance could be attributed to the synergistic effect of the enhanced carrier concentration and the Hall mobility related to the improved surface densification achieved with the electrospun ATO thin film and reduction of the residual In(OH)<sub>3</sub> phase by H<sub>2</sub> activation. Therefore, our method can be used as a novel strategy for obtaining high-performance solution-processed transparent conducting oxides at a low annealing temperature of 200 °C for use in various optoelectronic applications.

## 1. Introduction

Transparent conducting oxides (TCOs) exhibiting unique properties such as low resistivity ( $< 10^{-3} \Omega \text{ cm}$ ) and high transmittance ( $> 80\%$ ) are utilised as an important component in various state-of-the-art optoelectronic devices, including liquid crystal displays (LCDs), light emitting diodes (LEDs), touch screens, solar cells, and sensors [1–5]. Conventionally used TCOs include wide-bandgap oxide semiconductors such as Sn-doped In<sub>2</sub>O<sub>3</sub> (ITO), Sb-doped SnO<sub>2</sub> (ATO), and Al-doped ZnO (AZO) [6]. Among these, ITO, which is one of the most commonly used TCOs owing to its high transparency and low sheet resistance, is produced by vacuum-based deposition processes such as magnetron-sputtering, chemical vapor deposition, and vacuum evaporation, which require the use of sophisticated equipment and high vacuum conditions ( $< 10^{-4} \text{ Pa}$ ) [7]. Unfortunately, this makes TCOs very expensive, thereby limiting their use in broad industrial applications [8]. On the other hand, solution-based deposition processes have recently attracted attention as possible replacements of the vacuum processes. It is possible to fabricate film nanostructures using a simple and inexpensive method and coat materials with different geometries on large substrates or substrates via dip-coating, spin-coating, and

inkjet-printing [3,9,10]. For example, Lee et al. synthesised ITO electrodes by spin-coating an ITO nanocrystal (10.0 nm)-tetrabutylammonium hydroxide dispersion, thereby achieving a low sheet resistance of ~133.0 Ω/□ and a high transparency of ~88% at an annealing temperature of ~300 °C [11]. Chen et al. prepared uniform ITO electrodes using an acetylacetone-assisted sol-gel spin-coating process, achieving the good transparent conducting performances such as a sheet resistance of ~30.0 Ω/□ and optical transmittance of ~90.2% after performing annealing at 400 °C [8]. However, the improvement in the transparent conducting performances with the solution-based process is depends on the high annealing temperature and complicated chemical reactions (i.e. ethanolamine and combustion reaction) [12,13], which might limit the effective use of produced materials in large-scale and flexible applications in future industry, resulting in a decline of the price and performance competitiveness of the TCOs. Therefore, a study investigating the production of solution-processed TCOs at a low annealing temperature under 200 °C is important in terms of optoelectronic applications requiring low-cost fabrication and flexibility.

In this study, we fabricate transparent ITO/ATO electrodes by carrying out spin-coating of hybrid ITO nanoinks, electrospinning of

\* Corresponding author at: Program of Materials Science & Engineering, Convergence Institute of Biomedical Engineering and Biomaterials, Seoul National University of Science and Technology, Seoul 139-743, Republic of Korea.

E-mail address: [hjahn@seoultech.ac.kr](mailto:hjahn@seoultech.ac.kr) (H.-J. Ahn).

<http://dx.doi.org/10.1016/j.ceramint.2017.02.006>

Received 26 December 2016; Received in revised form 1 February 2017; Accepted 1 February 2017

Available online 04 February 2017

0272-8842/ © 2017 Elsevier Ltd and Techna Group S.r.l. All rights reserved.

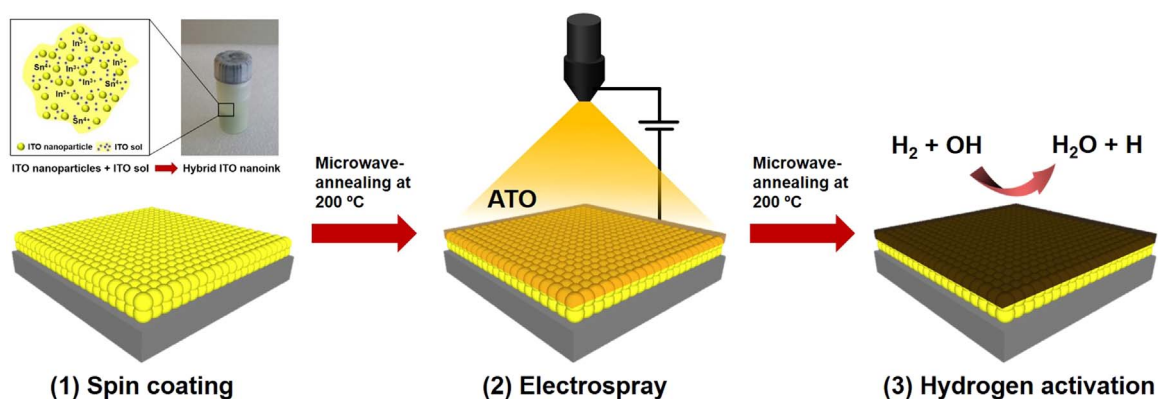


Fig. 1. Schematic diagram for fabricating  $H_2$ -activated ITO/ATO electrodes.

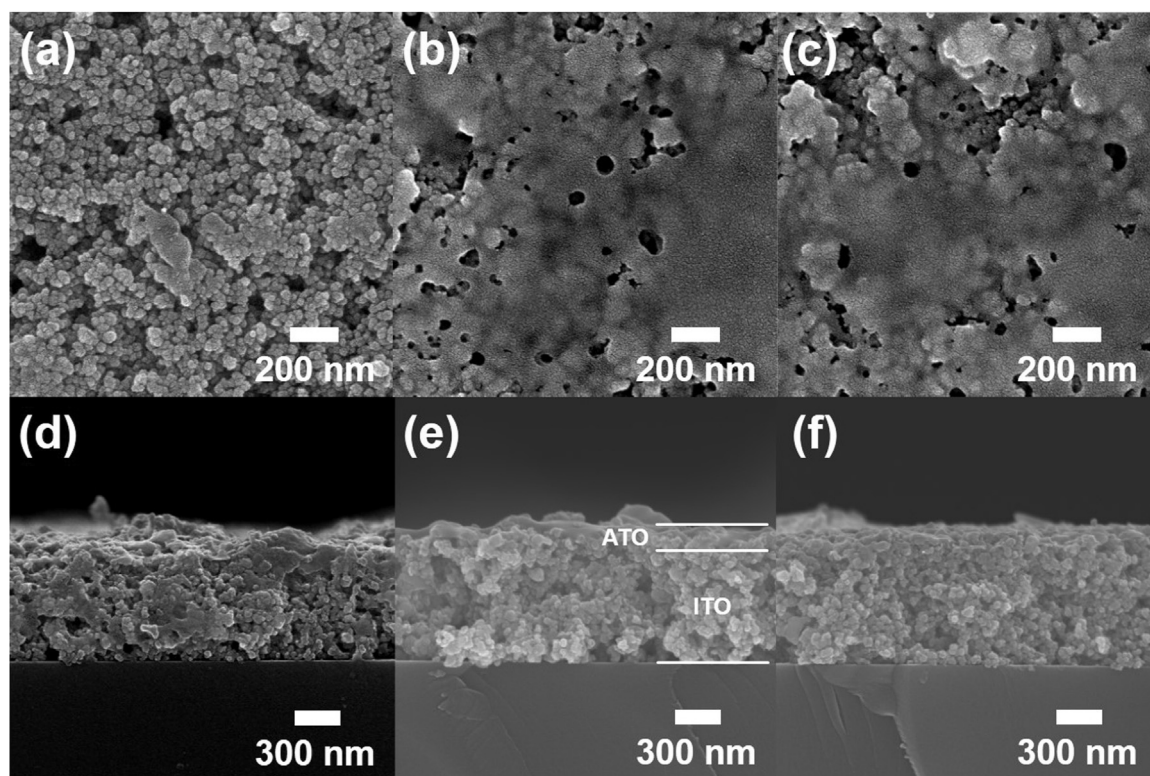


Fig. 2. (a-c) Top-view FESEM images and (d-f) cross-view FESEM images of ITO electrodes, ITO/ATO electrodes, and  $H_2$ -activated ITO/ATO electrodes, respectively.

ATO, and  $H_2$  activation at a low annealing temperature of 200 °C. In addition, we demonstrate the major mechanism involved in improving the transparent conducting performances at low annealing temperatures by examining the structural, chemical, electrical, and optical properties of the produced materials. For transparent ITO/ATO electrodes, the ATO thin films are used as a protection layer to prevent the loss of oxygen vacancies for ITO electrodes due to their good thermal stability, minimizing the decrease in electrical properties of the electrode during the annealing process.

## 2. Materials and methods

Transparent ITO/ATO electrodes were fabricated using a combined process of spin-coating, electro spray, and  $H_2$  activation. Fig. 1 represents the schematic of the process employed for fabricating  $H_2$ -activated ITO/ATO electrodes. Initially, ITO electrodes were prepared by spin-coating using hybrid ITO nanoinks, which are composed of highly crystalline ITO nanoparticles and an ITO sol with a weight ratio of 0.24, with microwave-

annealing (2.0 kW, UX-02, UNICREA) carried out at 200 °C. Since the ITO sol smoothly connects the empty space among the ITO nanoparticles, the hybrid nanoink can be effectively used for producing high-performance ITO electrodes with a low-temperature process [13]. Then, ATO was deposited by electro spraying on the prepared ITO electrodes in order to improve the transparent conducting performance. The solution for electro spray was prepared by dissolving tin (II) chloride dihydrate ( $SnCl_2 \cdot 2H_2O$ , Aldrich) and antimony chloride ( $SbCl_3$ , Aldrich) in 2-propanol. The molar ratio of Sn and Sb was fixed as 10:1 as previously reported [14]. The obtained transparent ATO solution was loaded into a syringe with a 23-gauge stainless-steel needle. For electro spraying, voltage and feeding rates of 24 kV and 0.03 ml/h, respectively, were employed. The distance between the needle and the collector was fixed as 10 cm. After performing microwave annealing at 200 °C, the prepared ITO/ATO electrodes were activated using  $H_2$  gas ( $N_2:H_2 = 90:10$ ) at 200 °C for 10 h, resulting in the production of  $H_2$ -activated ITO/ATO electrodes. Thus, we prepared three types of TCOs: ITO electrodes, ITO/ATO electrodes, and  $H_2$ -activated ITO/ATO electrodes.

The surface morphology of the electrodes was characterised using field-emission scanning electron microscopy (FE-SEM, Hitachi S-4800) and atomic force microscopy (AFM, diDimension™ 3100). The crystalline structure and chemical bonding state were analysed using X-ray diffraction (XRD, Rigaku D/Max-2500 diffractometer using Cu  $K_{\alpha}$  radiation) and X-ray photoelectron spectroscopy (XPS, ESCALAB 250 equipped with an Al  $K_{\alpha}$  X-ray source), respectively. The electrical and optical properties of the electrodes were measured using a Hall effect measurement system (Ecopia, HMS-3000) and UV–vis spectroscopy (Perkim-Elmer Lambda-35), respectively.

### 3. Results and discussion

Fig. 2(a–c) show the top-view FESEM images of the ITO electrodes, ITO/ATO electrodes, and  $H_2$ -activated ITO/ATO electrodes fabricated at 200 °C. For ITO electrodes, although the ITO sol acts as an important connecting link between the ITO nanoparticles, a rough surface morphology is observed due to the low annealing temperature, which might cause poor electrical properties with an increased grain boundary scattering on the electrode surface [15,16]. On the other hand, ITO/ATO electrodes exhibit a smooth surface morphology in which the ITO nanoparticles are covered with the electrospayed ATO thin film, and the deposition of the ATO thin film leads to a decrease in the pores and the inter-grain distance on the surface. This includes enhancements in the electrical properties of the TCO [17]. After performing  $H_2$  activation (Fig. 2(c)), the surface morphology of the  $H_2$ -activated ITO/ATO electrodes is unchanged, revealing no critical changes occurring as compared to that of the ITO/ATO electrodes. From the cross-view FESEM images shown in Fig. 2(d–f), the thickness values are measured to be ~814.5–933.7 nm for ITO electrodes, ~907.2–980.1 nm for ITO/ATO electrodes, and ~942.2–980.2 nm for  $H_2$ -activated ITO/ATO electrodes, indicating the successful deposition of the ATO thin film with an average thickness of ~61.6 nm on the ITO electrodes. While ITO electrodes exhibit a rough surface morphology due to the formation of pores (Fig. 2(d)), the other ITO electrodes deposited with ATO thin films exhibit a smooth surface morphology with enhanced densification (Fig. 2(e) and (f)). Therefore, the introduction of ATO thin films might cause improvements in electrical properties of the solution-processed TCOs obtained at a low annealing temperature of 200 °C [17].

In order to further analyse the effect of the presence of the electrospayed ATO thin film on the ITO electrodes, AFM analysis of the ITO electrodes and ITO/ATO electrodes was carried out (Fig. 3(a) and (b), respectively). The root mean square roughness ( $R_{ms}$ ) is defined as the standard deviation of height observed on the electrode surface,

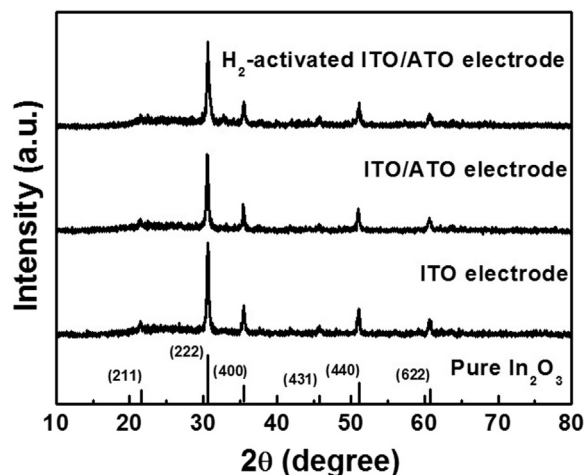


Fig. 4. XRD plots of all the electrodes fabricated at annealing temperature of 200 °C.

which is directly related to surface densification that affects the transparent conducting performance [18]. That is, with a decrease in the surface roughness, a significant enhancement on surface densification of the electrode can be achieved, resulting in improving the electrical properties such as Hall mobility of TCOs [13].  $R_{ms}$  is measured to be ~31.0 nm for the ITO electrodes and ~24.5 nm for the ITO/ATO electrodes. The surface densification of ITO electrodes is enhanced on filling the ITO inter-grains with the ATO thin films. This results in shortening of the transport distance of electrons by achieving a smooth connection among the ITO nanoparticles, resulting in the alleviation of grain-boundary scattering at the surface of TCO [19].

Fig. 4 shows the XRD patterns obtained for all electrodes. All the electrodes exhibit the main characteristic diffraction peaks at 21.66° and 35.54°, which can be assigned to the (222) and (400) planes of polycrystalline  $In_2O_3$  with a cubic bixbyite structure (space group Ia3 [206]; JCPDS card No. 06–0416). As compared to the XRD pattern of the pure  $In_2O_3$  shown at the bottom (30.60° for (200) plane and 35.49° for (400) plane), the observed characteristic diffraction peaks of the electrodes are slightly shifted toward higher diffraction angles. Thus, the ITO phase is successfully formed by doping  $Sn^{4+}$  into the  $In_2O_3$  lattice due to the smaller ionic radius of  $Sn^{4+}$  (0.69 Å) than that of  $In^{3+}$  (0.80 Å), which can be explained by Bragg's equation ( $n\lambda = 2d \sin\theta$ ) [20]. In addition, no diffraction peaks corresponding to the ATO phase are observed in the XRD patterns, suggesting the formation of

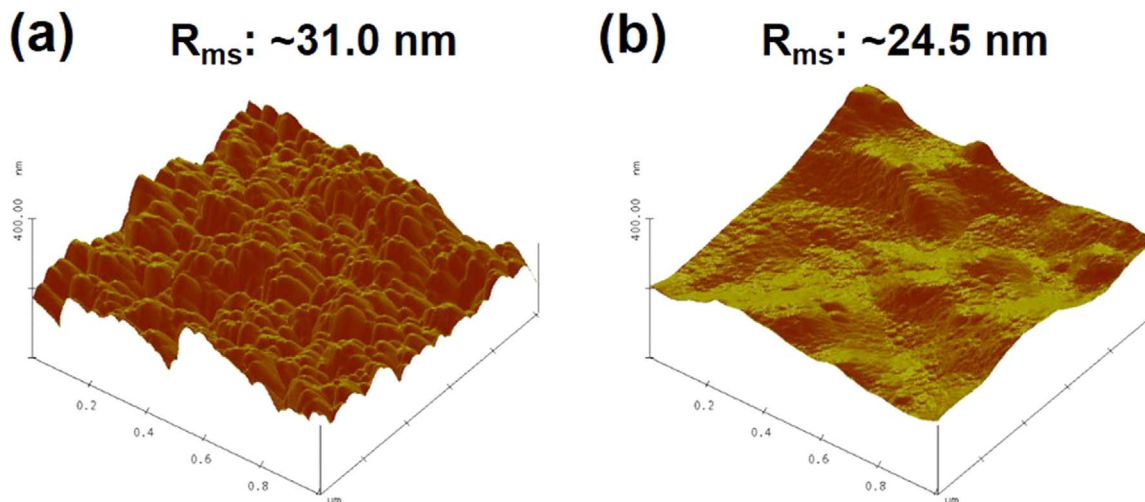


Fig. 3. AFM images obtained from (a) ITO electrodes and (b) ITO/ATO electrodes.

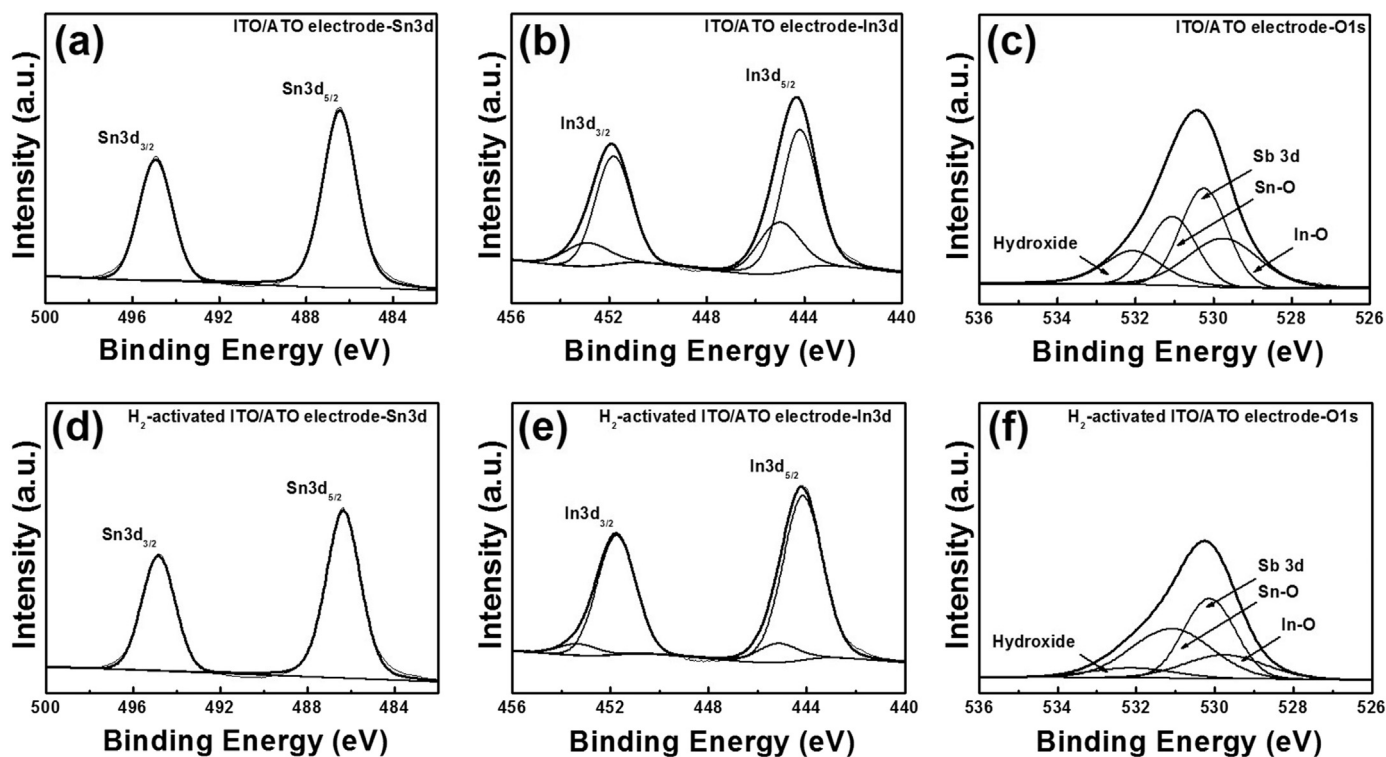


Fig. 5. XPS core-level spectra of Sn 3d, In 3d, and O 1 s obtained from (a-c) ITO/ATO electrodes and (d-f) H<sub>2</sub>-activated ITO/ATO electrodes, respectively.

amorphous phases due to insufficient crystallisation temperature (230–250 °C) [21]. In addition, H<sub>2</sub>-activated ITO/ATO electrodes exhibit similar diffraction peaks as those exhibited by other electrodes, indicating that no secondary phases are formed.

In order to further investigate the effect of H<sub>2</sub> activation on the electrodes, XPS measurements were carried out. Fig. 5 shows the Sn3d, In3d, and O1s XPS core-level spectra of ITO/ATO electrodes and H<sub>2</sub>-activated ITO/ATO electrodes. All the binding energies were calibrated using the C1s (284.5 eV). For both the electrodes as shown in Fig. 5(a) and (d), the dominant Sn3d<sub>5/2</sub> and Sn3d<sub>3/2</sub> peaks are observed at ~486.3 eV and ~494.8 eV, respectively, indicating the presence of Sn<sup>4+</sup> ions in SnO<sub>2</sub>. In addition, the dominant peaks corresponding to In3d<sub>5/2</sub> and In3d<sub>3/2</sub> (Fig. 5(b) and (e)) are observed at ~444.1 eV and ~451.7 eV, respectively, indicating the presence of In<sup>3+</sup> ions in In<sub>2</sub>O<sub>3</sub>, implying the successful formation of crystalline ITO phases [13]. The additional peaks corresponding to In3d photoelectrons are observed at ~445.4 eV for In 3d<sub>5/2</sub> and ~453.3 eV for In 3d<sub>3/2</sub>, indicating to the formation of In(OH)<sub>3</sub> due to the low annealing temperature [22].

Interestingly, the ratio of the peak areas for the In<sub>2</sub>O<sub>3</sub> phase to the In(OH)<sub>3</sub> phase is evidently increased after H<sub>2</sub> activation. In general, the conversion of In(OH)<sub>3</sub> to In<sub>2</sub>O<sub>3</sub> occurs at an annealing temperature above ~250 °C [23]. However, despite the low annealing temperature of 200 °C employed with the microwave annealing process, H<sub>2</sub> activation leads to the formation of In<sub>2</sub>O<sub>3</sub> through H<sub>2</sub>O desorption induced by the decomposition of hydroxides (H<sub>2</sub>+OH→H<sub>2</sub>O+H), which might affect the electrical properties of the electrodes thanks to the reduction of the residual In(OH)<sub>3</sub> phase [24,25]. The O 1 s XPS peaks shown in Fig. 5(c) and (f) are decomposed into four different components at ~529.7 eV, ~530.2 eV, ~531.0 eV, and ~531.0 eV. The first and third peaks are associated with In-O and Sn-O bonds, respectively [13]. The second peak originates from the Sb 3d group, indicating to the formation of ATO [15]. The fourth peak associated with hydroxide indicates a remarkable decrease in the peak area observed after H<sub>2</sub> activation, in agreement with the XPS results obtained for In3d photoelectrons, revealing conversion of In(OH)<sub>3</sub> to In<sub>2</sub>O<sub>3</sub>. This confirms the successful formation of crystalline ITO phases and ATO

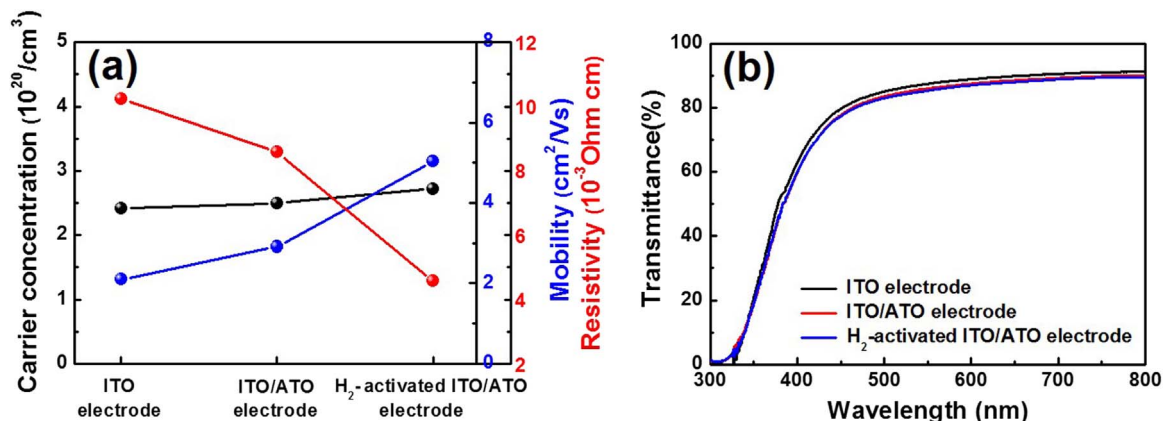


Fig. 6. (a) Electrical properties and (b) optical transmission curve of all the electrodes.

**Table 1**

Summary of electrical and optical properties obtained from all the electrodes.

|   | ITO electrode           | ITO/ATO electrode       | H <sub>2</sub> -activated ITO/ATO electrode |
|---|-------------------------|-------------------------|---|
| Carrier concentration (cm <sup>-3</sup> ) | 2.42 × 10 <sup>20</sup> | 2.50 × 10 <sup>20</sup> | 2.72 × 10 <sup>20</sup>                     |
| Hall mobility (cm <sup>2</sup> /(V s))    | 2.10                    | 2.91                    | 5.03  |
| Resistivity (Ω·cm)                        | 1.23 × 10 <sup>-2</sup> | 8.58 × 10 <sup>-3</sup> | 4.57 × 10 <sup>-3</sup>                     |
| Sheet resistance (Ω/□)                    | 140.2                   | 90.9                    | 47.5  |
| Transmittance (% at 550 nm)               | 87.6                    | 86.1                    | 85.3  |

**Table 2**

List of sheet resistance and transmittance for the solution-based ITO electrodes obtained from various solution-based processes.

| Processes       | Sheet resistance (Ω/□) | Transmittance (% at 550 nm) | Annealing temperature (°C) | References |
|-----------------|------------------------|-----------------------------|----------------------------|------------|
| Inkjet-printing | ~202                   | ~88                         | 450                        | [3]        |
| Inkjet-printing | ~517                   | ~87                         | 400                        | [30]       |
| Spin-coating    | ~30                    | ~90                         | 550                        | [29]       |
| Spin-coating    | ~30                    | ~90                         | 400                        | [8]        |
| Spin-coating    | ~270                   | ~80                         | 530                        | [7]        |
| Spin-coating    | ~130                   | ~88                         | 300                        | [10]       |
| Spin-coating    | ~466                   | ~90                         | 300                        | [11]       |
| Our works       | ~47                    | ~85                         | 200                        | –          |

phases on H<sub>2</sub>-activated ITO/ATO electrodes despite the use of low annealing temperature at 200 °C.

Fig. 6(a) shows the electrical properties of the electrodes, including the carrier concentration, Hall mobility, and resistivity. ITO electrodes exhibit a carrier concentration of  $\sim 2.42 \times 10^{20} \text{ cm}^{-3}$  and Hall mobility of  $\sim 2.10 \text{ cm}^2/(\text{Vs})$ . After the deposition of the electro-sprayed ATO thin film on the ITO electrodes (ITO/ATO electrodes), the carrier concentration is unchanged ( $\sim 2.50 \times 10^{20} \text{ cm}^{-3}$ ); however, the Hall mobility is increased to  $\sim 2.91 \text{ cm}^2/(\text{Vs})$ , which is induced by the decreased grain-boundary scattering resulting from the improved surface densification achieved with the ATO thin film [19]. The H<sub>2</sub>-activated ITO/ATO electrodes exhibit the highest carrier concentration ( $\sim 2.72 \times 10^{20} \text{ cm}^{-3}$ ) and Hall mobility ( $\sim 5.03 \text{ cm}^2/(\text{Vs})$ ) as compared to the previously reported values. This is attributed to the reduction of the residual In(OH)<sub>3</sub> phase achieved with H<sub>2</sub> activation, offering more free electrons and an efficient pathway for carrier movement [26,27]. Based on the carrier concentration (*N*) and Hall mobility (*μ*), the resistivity (*ρ*) can be calculated using the following equation [14]:

$$\rho = 1/(Ne\mu) \quad (1)$$

, where *N* is the carrier concentration, *e* is electron charge ( $1.602 \times 10^{-19} \text{ C}$ ), and *μ* is the Hall mobility. Thus, the resistivity of the electrode is calculated to be  $\sim 12.3 \times 10^{-3} \text{ Ω}\cdot\text{cm}$  for ITO electrodes,  $\sim 8.58 \times 10^{-3} \text{ Ω}\cdot\text{cm}$  for ITO/ATO electrodes,  $\sim 4.57 \times 10^{-3} \text{ Ω}\cdot\text{cm}$  for H<sub>2</sub>-activated ITO/ATO electrodes. In addition, the sheet resistance (*R<sub>sh</sub>*) values can be calculated from the resistivity values using the corresponding values of thickness of the electrodes. The sheet resistance values are calculated to be  $\sim 140.2 \text{ Ω}/\square$  for ITO electrodes,  $\sim 90.9 \text{ Ω}/\square$  for ITO/ATO electrodes, and  $\sim 47.5 \text{ Ω}/\square$  for H<sub>2</sub>-activated ITO/ATO electrodes. This indicates that the H<sub>2</sub>-activated ITO/ATO electrodes exhibit significantly higher electrical properties as compared to other electrodes despite the use of the low annealing temperature of 200 °C. The performance improvement could be attributed to the enhanced carrier concentration and Hall mobility of the electrodes, which is induced via the synergistic effect of increased surface densification with the presence of electro-sprayed ATO thin film and the reduction of the residual In(OH)<sub>3</sub> phase with H<sub>2</sub> activation. In addition, this might affect the optical properties of the electrodes. Fig. 6(b) shows the optical transmittance curves obtained for the electrodes. In general, an increase in the thickness of the TCO results in a decrease of the optical transmittance (*T*) at 550 nm [28]. However, with the introduction of the electro-sprayed ATO thin

film and H<sub>2</sub> activation, the optical transmittance of the electrodes is unchanged ( $\sim 87.6\%$  for ITO electrodes,  $\sim 86.1\%$  for ITO/ATO electrodes, and  $\sim 85.3\%$  for H<sub>2</sub>-activated ITO/ATO electrodes) due to the alleviation of light scattering in the electrodes [12,27]. Based on the electrical and optical properties obtained (shown in Table 1), we calculated the Figure of merit (FOM,  $T^{10}/R_{sh}$ ) that evaluates the transparent conducting performance [8]. The FOM value is calculated to be  $\sim 1.8 \times 10^{-3} \text{ Ω}^{-1}$  for ITO electrodes,  $\sim 2.6 \times 10^{-3} \text{ Ω}^{-1}$  for ITO/ATO electrodes, and  $\sim 4.2 \times 10^{-3} \text{ Ω}^{-1}$  for H<sub>2</sub>-activated ITO/ATO electrodes. Thus, the H<sub>2</sub>-activated ITO/ATO electrodes exhibit the highest transparent conducting performance owing to their low sheet resistance ( $\sim 47.5 \text{ Ω}/\square$ ) and good optical transmittance ( $\sim 85.3\%$ ). The previously reported values indicating the electrical and optical properties of solution-processed ITO electrodes are shown in Table 2 [3,7,8,11,12,30,31]. These studies were carried out with annealing performed processes at high temperatures (300–550 °C) or complex chemical reactions for achieving a high performance with the solution-processed ITO electrodes. The H<sub>2</sub>-activated ITO/ATO electrodes produced in this study exhibit superior electrical and optical properties despite the use of the low annealing temperature of 200 °C. Thus, the development of solution-processed H<sub>2</sub>-activated ITO/ATO electrodes at 200 °C can be employed for fabricating attractive TCOs for use in potential optoelectronic applications owing to the advantages such as flexibility and low-cost.

#### 4. Conclusion

Transparent ITO/ATO electrodes were fabricated by spin-coating, electro-spray, and H<sub>2</sub> activation at a low annealing temperature of 200 °C. The electro-sprayed ATO thin films exhibit a smooth surface morphology, which might cause an improvement in surface densification associated with the short transport distance of electrons. In particular, after performing H<sub>2</sub> activation at 200 °C, the In(OH)<sub>3</sub> phases formed at low annealing temperatures are converted to ITO with H<sub>2</sub>O desorption resulting from the decomposition of hydroxide by H<sub>2</sub> activation. Thus, H<sub>2</sub>-activated ITO/ATO electrodes exhibit outstanding sheet resistance ( $\sim 47.5 \text{ Ω}/\square$ ) and good transmittance ( $\sim 85.3\%$ ) properties despite the use of the low annealing temperature of 200 °C. The improvements in the performance can be attributed to the increased carrier concentration and Hall mobility, induced via the synergistic effect of improved surface densification achieved with the

presence of the electrosprayed ATO thin film on the ITO electrode and the reduction of the residual  $\text{In}(\text{OH})_3$  phase resulting from  $\text{H}_2$  activation. These results indicate that the  $\text{H}_2$ -activated ITO/ATO electrodes may be used in potential TCOs for optoelectronic applications demanding low-temperature fabrication and flexibility.

## Acknowledgements

This work was supported by Grant No. 10067693 from the Ministry of Knowledge Economy (MKE) and the Fundamental R & D Program for Core Technology of Materials funded by the Ministry of Knowledge Economy, Republic of Korea.

## References

- [1] C.J. Brabec, Organic photovoltaics: technology and market, *Sol. Energy Mater. Sol. Cells* 83 (2004) 273–292.
- [2] N. Ameera, A. Shuhaimi, N. Surani, M. Rusop, M. Hakim, M.H. Mamat, M. Mansor, M. Sobri, V. Ganesh, Y. Yusuf, Nanocolumnar zinc oxide as a transparent conductive oxide film for a blue InGaN-based light emitting diode, *Ceram. Int.* 41 (2015) 913–920.
- [3] J.-A. Jeong, J. Lee, H. Kim, H.-K. Kim, S.-I. Na, Ink-jet printed transparent electrode using nano-size indium tin oxide particles for organic photovoltaics *Sol. Energy Mater. Sol. Cells* 94 (2010) 1840–1844.
- [4] H.-K. Kim, S. Lee, K.-S. Yun, Capacitive tactile sensor array for touch screen application, *Sens. Actuators A-Phys.* 165 (2011) 2–7.
- [5] Q. Wan, T.H. Wang, Single-crystalline Sb-doped  $\text{SnO}_2$  nanowires: synthesis and gas sensor application, *Chem. Commun.* (2005) 3841–3843.
- [6] T. Minami, Transparent conducting oxide semiconductors for transparent electrodes, *Semicond. Sci. Technol.* 20 (2005) S35–S44.
- [7] T.O.L. Sunde, E. Garskaite, B. Otter, H.E. Fossheim, R. Saeterli, R. Holmestad, M.-A. Einarsrud, T. Grande, Transparent and conducting ITO thin films by spin coating of an aqueous precursor solution, *J. Mater. Chem.* 22 (2012) 15740–15749.
- [8] Z. Chen, W. Li, R. Li, Y. Zhang, G. Xu, H. Cheng, Fabrication of Highly transparent and Conductive Indium-tin oxide thin films with a high figure of merit via solution processing, *Langmuir* 29 (2013) 13836–13842.
- [9] B.-R. Koo, H.-J. Ahn, Chemical properties of electrosprayed antimony tin oxide thin film/Ag nanowire multilayer for transparent conductive electrodes, *Appl. Phys. Express* 7 (2014) 075002.
- [10] J. Lee, M.A. Petruska, S. Sun, Surface modification and assembly of transparent indium tin oxide nanocrystals for enhanced conductivity, *J. Phys. Chem. C* 118 (2014) 12017–12021.
- [11] Z. Chen, X. Qin, T. Zhou, X. Wu, S. Shao, M. Xie, Z. Cui, Ethanolamine-assisted synthesis of size-controlled indium tin oxide nanoinks for low temperature solution deposited transparent conductive films, *J. Mater. Chem. C* 3 (2015) 11464–11470.
- [12] M.-G. Kim, M.G. Kanatzidis, A. Facchetti, T.J. Marks, Low-temperature fabrication of high-performance metal oxide thin-film electronics via combustion processing, *Nat. Mat.* 10 (2011) 382–388.
- [13] B.-R. Koo, H.-J. Ahn, Effect of hybrid nanoinks on solution-based Sn-doped  $\text{In}_2\text{O}_3$  films under low-temperature microwave annealing, *Ceram. Int.* 42 (2016) 509–517.
- [14] B.-R. Koo, H.-J. Ahn, Structural, electrical, and optical properties of Sb-doped  $\text{SnO}_2$  transparent conductive oxides fabricated using an electrospray technique, *Ceram. Int.* 40 (2014) 4375–4381.
- [15] H.-R. An, C.Y. Kim, S.-T. Oh, H.-J. Ahn, Effect of sol-layers on Sb-doped  $\text{SnO}_2$  thin films as solution-based transparent conductive oxides, *Ceram. Int.* 40 (2014) 385–391.
- [16] J. Steinhauser, S. Fay, N. Oliveira, E. Vallat-Sauvain, C. Ballif, Transition between grain boundary and intragrain scattering transport mechanisms in boron-doped zinc oxide thin films, *Appl. Phys. Lett.* 90 (2007) 142107.
- [17] N. Al-Dahoudi, M.A. Aegerter, Comparative study of transparent conductive  $\text{In}_2\text{O}_3:\text{Sn}$  (ITO) coatings made using a sol and a nanoparticle suspension, *Thin Solid Films* 502 (2006) 193–197.
- [18] D. Raoufi, A. Kiasatpour, H.R. Fallah, A.S.H. Rozatian, Surface characterization and microstructure of ITO thin films at different annealing temperatures, *Appl. Surf. Sci.* 253 (2007) 9085–9090.
- [19] M. Higuchi, M. Sawada, Y. Kuronuma, Microstructure and electrical characteristics of sputtered indium tin oxide films, *J. Electrochem. Soc.* 140 (1993) 1773–1775.
- [20] J. Lee, S. Lee, G. Li, M.A. Petruska, D.C. Paine, S. Sun, A facile solution-phase approach to transparent and conducting ITO nanocrystal assemblies, *J. Am. Chem. Soc.* 134 (2012) 13410–13414.
- [21] S. Muranaka, Y. Bando, T. Takada, Influence of substrate temperature and film thickness on the structure of reactively evaporated  $\text{In}_2\text{O}_3$  films, *Thin Solid Films* 151 (1987) 355–364.
- [22] R. Bayón, C. Maffiotte, J. Herrero, Chemical bath deposition of indium hydroxy sulphide thin films: process and XPS characterization, *Thin Solid Films* 353 (1999) 100–107.
- [23] A. Shanmugasundaram, B. Ramireddy, P. Basak, S.V. Manorama, S. Srinath, Hierarchical  $\text{In}(\text{OH})_3$  as a precursor to mesoporous  $\text{In}_2\text{O}_3$  nanocubes: a facile synthesis route, mechanism of self-Assembly, and enhanced sensing response toward hydrogen, *J. Phys. Chem. C* 118 (2014) 6909–6921.
- [24] J. Chen, X. Xu, X. Xu, D.H. Zhang, A global potential energy surface for the  $\text{H}_2+\text{OH} \leftrightarrow \text{H}_2\text{O}+\text{H}$  reaction using neural networks, *J. Chem. Phys.* 138 (2013) 154301.
- [25] E. Nishimura, M. Ando, K.-I. Onisawa, M. Takabatake, T. Minemura, Structural change during annealing of amorphous indium-tin oxide films deposited by sputtering with  $\text{H}_2\text{O}$  addition, *Jpn. J. Appl. Phys.* 35 (1996) 2788–2792.
- [26] H. Morikawa, M. Fujita, Crystallization and electrical property change on the annealing of amorphous indium-oxide and indium-tin-oxide thin films, *Thin Solid Films* 359 (2000) 61–67.
- [27] B. Yaglioglu, Y.-J. Huang, H.-Y. Yeom, D.C. Paine, A study of amorphous and crystalline phases in  $\text{In}_2\text{O}_3$ -10 wt% ZnO thin films deposited by DC magnetron sputtering, *Thin Solid Films* 496 (2006) 89–94.
- [28] L. Hao, X. Diao, H. Xu, B. Gu, T. Wang, Thickness dependence of structural, electrical and optical properties of indium tin oxide (ITO) films deposited on PET substrates, *Appl. Surf. Sci.* 254 (2008) 3054–3508.
- [29] M.J. Alam, D.C. Cameron, Optical and electrical properties of transparent conductive ITO thin films deposited by sol-gel process, *Thin Solid Films* 00 (2000) 455–459.
- [30] N.-R. Kim, J.-H. Lee, Y.-Y. Lee, D.-H. Nam, H.-W. Yeon, S.-Y. Lee, T.-Y. Yang, Y.-J. Lee, A. Chu, K.T. Nam, Y.-C. Joo, Enhanced conductivity of solution-processed indium tin oxide nanoparticle films by oxygen partial pressure controlled annealing, *J. Mater. Chem. C* 1 (2013) 5953–5959.
- [31] M.-S. Hwang, B.-Y. Jeong, J. Moon, S.-K. Chun, J. Kim, Inkjet-printing of indium tin oxide (ITO) films for transparent conducting electrodes, *Mater. Sci. Eng. B* 176 (2011) 1128–1131.